Photon Tunneling Contributions for Laboratory-Grown Hexagonal Columns

D. L. Mitchell and W. P. Arnott
Desert Research Institute
Division of Atmospheric Sciences
Reno, Nevada

C. Schmitt
SPEC, Inc.
Boulder, Colorado

Introduction

Ice particle-radiation interactions differ from cloud droplet-radiation interactions due to differences in (1) phase functions; (2) the relationships between particle dimension, area, and mass; and (3) photon tunneling effects (e.g., Nussenzveig 1977; Guimaraes and Nussenzveig 1992). Tunneled radiation here can be viewed as non-incident radiation beyond a particle's physical cross section, which would be absorbed if the particle were a black body. Another type of tunneling is referred to as edge effects that manifest as surface waves. These do not enter the particle's interior and are not absorbed, but are responsible for large angle diffraction (Mitchell 2000). Although the physical reasons remain unclear, tunneling depends on ice particle morphology, such as aspect ratio, and its contribution to absorption in ice crystals is less than for spheres (Baran et al. 1998). Francis et al. (1999) provided evidence that tunneling at 8.5 μm and 11.1 μm in a cirrus deck sampled microphysically and radiometrically was negligible. The absence of tunneling effects in ice crystals would reduce their absorption efficiency in the thermal infrared (IR) by typically 20%, although in the far IR this reduction (relative to tunneling predicted by Mie theory) can be up to 43%. Hence, IR remote sensing is plagued with large uncertainties until the role of tunneling in ice is resolved.

We present estimates of the contribution of photon tunneling for hexagonal columns, as determined from Fourier-transform interferometric radiometer (FTIR) measurements of optical depth in a laboratory ice cloud and corresponding ice particle size spectra. The tunneling contribution to extinction and absorption is evaluated by means of a tunneling factor, which determines the fraction of the Mie tunneling terms to be utilized (Mitchell 2000).

FTIR Extinction Measurements

A laboratory experiment was conducted whereby tunneling was investigated using a FTIR exhibiting a wavelength range of 2 μm to 18 μm, which sampled an ice cloud grown in a chamber, with hexagonal column ice crystals having maximum dimensions $D < 40$ μm. Size distributions (SD) exhibited a mean D of about 14 μm (Figure 1). Defining effective diameter (D_{eff}) as

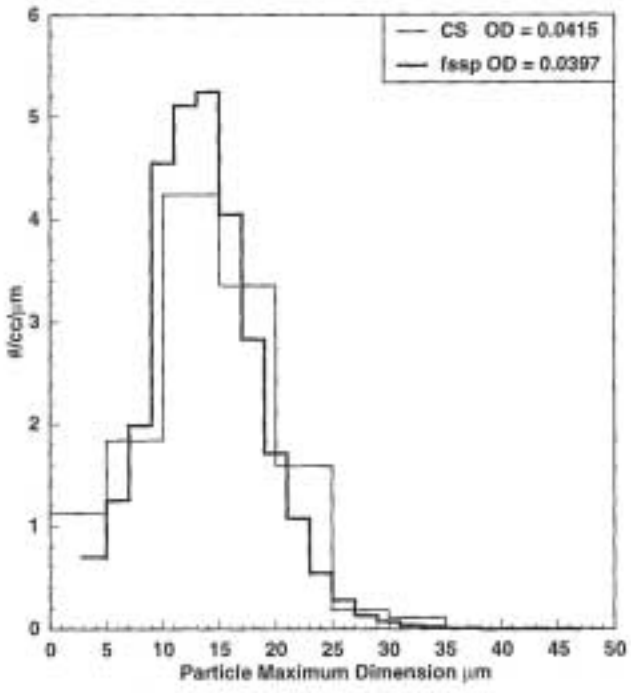

Figure 1. Hexagonal column size distributions measured by the forward scattering spectrometer probe (FSSP) and Cloudscope within the Desert Research Institute (DRI) cloud chamber.

$$D_{eff} = 3/2\ (V_t / P_t), \tag{1}$$

where V_t and P_t = SD volume and projected area, with V_t referenced to the density of bulk ice (0.92 g cm^{-3}), D_{eff} was around 14 μm. Since tunneling is most pronounced when the wavelength λ and D_{eff} are similar (Mitchell 2000), the range of λ and D_{eff} used here are well suited for evaluating tunneling contributions to extinction and absorption.

The basic experimental design (Arnott et al. 1995; Schmitt and Arnott 1999) consists of a laser at 0.685 μm that penetrates an ice cloud grown within a chamber over the same path as the FTIR beam. Ideally, the ice crystals would be large enough such that the extinction efficiency for the laser ($Q_{ext,\,l}$) equals 2.00. From the FTIR optical depth (τ_{obs}) and the laser optical depth (τ_l), the measured infrared extinction efficiency, $Q_{ext,obs}$, is normally calculated as

$$Q_{ext,obs} = Q_{ext,\,l}\ (\tau_{obs}/\tau_l). \tag{2}$$

Since tunneling contributes to Q_{ext} as a function of size parameter x ($x = \pi D_{eff}/\lambda$, λ = wavelength) and refractive index, $Q_{ext,obs}$ can be used to estimate the amount of tunneling exhibited by ice crystals. Unfortunately, the laser malfunctioned during the experimental runs for hexagonal columns, making it necessary to substitute τ_l in Eq. (2) with the τ measured by the FTIR at λ = 2.00 μm. Since D_{eff} was about 14 μm, x is about 22 when λ = 2.00 μm. Fortunately, at this x and refractive index, tunneling

contributions are relatively low, making it feasible to use the measured τ at 2.00 μm to estimate tunneling contributions at longer wavelengths. However, tunneling contributions at x = 22 are not negligible, and $Q_{ext,obs}$ was estimated as

$$Q_{ext,obs} = Q_{ext,\ 2\ \mu m}\ (\tau_{obs}/\tau_{obs,\ 2\ \mu m}) \quad (3)$$

Since it could not be assumed $Q_{ext,2\ \mu m} = 2$ at x = 22, $Q_{ext,2\ \mu m}$ was calculated from the measured SD (Mitchell 1998, 2000), as described later under Method 2.

To compare $Q_{ext,obs}$ with those predicted (Q_{ext}), SD were measured in the cloud chamber about 30 cm above the FTIR using two instruments: an FSSP and a Cloudscope (CS) (Schmitt and Arnott 1999). Both the CS and FSSP measure D down to about 3 μm. The Cloudscope's operating principle is impaction, and concentrations were corrected for changes in collection efficiency (Schmitt and Arnott 1999). Size spectra obtained from 11 experiment runs (15 seconds per run) exhibiting similar τ_{obs} were averaged together, giving a mean SD for each instrument. These mean SDs from the CS and FSSP were similar, and are shown in Figure 1, giving confidence that the SDs were accurately measured. From both SDs, predicted values of Q_{ext} were obtained by integrating bin-by-bin to obtain the extinction coefficient (Mitchell 1998, 2000). This coefficient was then divided by the SD projected area (assuming random orientation) using the area-dimensional relations (Mitchell et al. 1996), thus giving Q_{ext} for the SD. The CS video records the ice crystal shapes, which were hexagonal columns throughout this experiment.

Estimating the Tunneling Contribution

Estimates of tunneling amounts can be obtained from the radiation scheme of Mitchell (1998), whereby ice crystals are converted to equivalent photon path spheres, d_e, as defined by Eq. (1), where P and V now refer to an individual crystal. In this scheme, the tunneling processes are parameterized, as well as the processes of internal reflection/refraction, while extinction due to geometrical blocking, diffraction, and interference is represented through the anomalous diffraction approximation (ADA). Using ice and water spheres, this scheme agrees with Mie theory within 10% for Q_{ext} for size parameters x > 1.0, based on the treatment for single particles. Tunneling was quantified as a "tunneling factor," or t_f, ranging from 0 to 1.0, where 0 and 1.0 correspond to (ADA + internal reflection/refraction) and Mie theory, respectively. In our radiation scheme (Mitchell 1998, 2000), the tunneling terms are multiplied by t_f to give tunneling contributions for a given crystal shape.

From Eq. (3), when λ = 2.00 μm, $Q_{ext,obs} = Q_{ext,\ 2\ \mu m}$. For the conditions here, tunneling contributions tend to increase as λ increases beyond 2 μm (Figure 2). The solid upper curve is $Q_{ext,obs}$. $Q_{ext,obs}$ is not reported over λ regions exhibiting absorption by water vapor. The $Q_{ext,obs}$ for λ > 14.2 μm may also be slightly overestimated due to CO_2 absorption, although this interference is weak compared to the water vapor bands. We have included this data in our analysis. The two dashed curves give Q_{ext} predicted from the two mean SDs measured via the CS and FSSP. These predicted curves assume zero tunneling ($t_f = 0$). Hence, the difference between the predicted and measurement derived Q_{ext} curves should be primarily due to tunneling. Regarding $Q_{ext,obs}$, $Q_{ext,\ 2\ \mu m}$ was calculated assuming $t_f = 0$, so that Q_{ext}

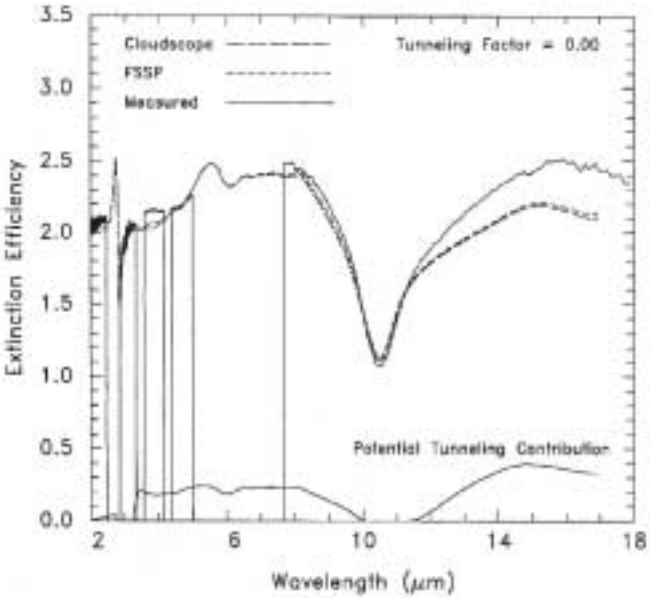

Figure 2. Predicted Q_{ext} from the CS and FSSP for $t_f = 0$, contrasted with measured Q_{ext}. Lower curve gives the maximum potential tunneling contribution for $t_f = 1.0$.

predicted and $Q_{ext,obs}$ are identical at $\lambda = 2.00$ μm. Hence, differences between the Q_{ext} and $Q_{ext,obs}$ curves should be due to tunneling contributions over and above those corresponding to $\lambda = 2.00$ μm. Also shown by the lower solid curve are the maximum predicted tunneling contributions from the SDs ($t_f = 1.0$), which is only the contribution that exceeds that predicted for $\lambda = 2.00$ μm. If hexagonal columns exhibited the same degree of tunneling as ice spheres, adding the potential tunneling contribution (lower curve) to the predicted curves should match the $Q_{ext,obs}$ curve.

Method 1

Method 1 evaluates tunneling in the λ region where contributions are greatest. The largest tunneling contribution in Figure 2, from both theory and measurements, occurs for $\lambda > 14$ μm. Since CO_2 absorption at $\lambda > 14$ μm may artificially enhance Q_{ext} to a small extent, tunneling was evaluated at $\lambda = 14$ μm. By calculating the ratio $Q_{ext,obs}/Q_{ext,predicted}$ at $\lambda = 14$ μm for a given t_f, and incrementing t_f from 0 to 1.0, a spectrum of Q_{ext} ratios are generated (Figure 3). A Q_{ext} ratio of 1.0 indicates the tunneling factor appropriate for hexagonal columns. A minor process contributing to tunneling is known as edge effects, and it is unclear whether edge effects occur in ice crystals. Figure 3 indicates that regardless of edge effects, a tunneling factor of 0.8 appears appropriate for hexagonal columns in this experiment. Figure 4 compares Q_{ext} predicted from each mean SD with $Q_{ext,obs}$ from Eq. (3), based on a tunneling factor of 0.80. While agreement between theory and observation appears excellent for $\lambda > 8$ μm (differences for $\lambda > 15$ μm are probably due to CO_2 absorption), agreement is not as good for $\lambda < 8$ μm. Therefore, a second method based on all λ's is also used.

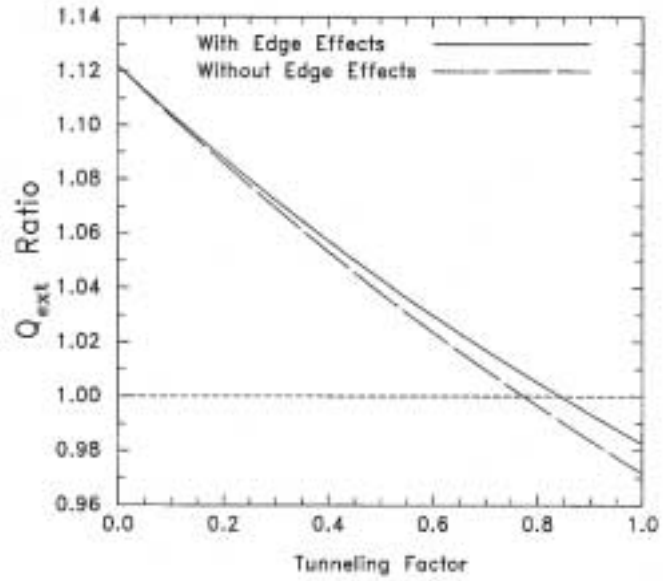

Figure 3. Observed-to-predicted Q_{ext} ratio evaluated at λ = 14 μm over the range of possible t_f values. A ratio of unity gives the t_f at λ = 14 μm.

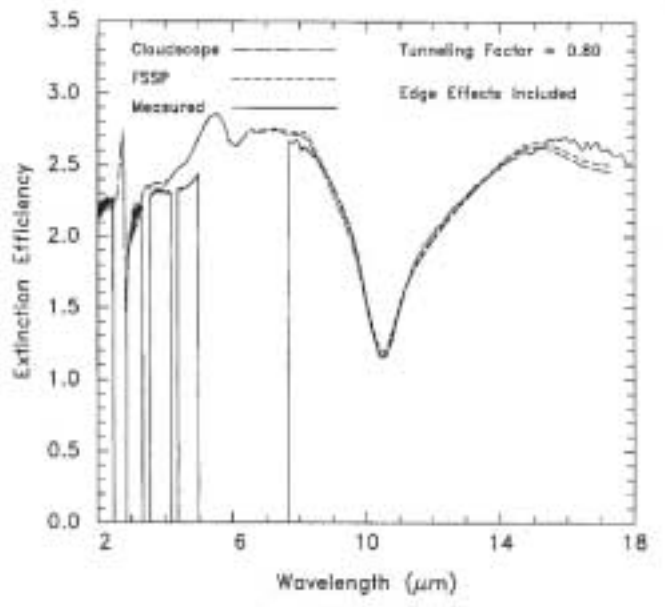

Figure 4. Comparison of measured and predicted Q_{ext} for t_f = 0.80, which minimizes differences at λ = 14 μm where tunneling contributions are highest.

Method 2

A program that minimizes errors between measured and predicted Q_{ext} values at all λ values was created, whereby t_f is varied. The radiation scheme requires knowledge of an ice crystal's mass (=> V) and projected area P, which were estimated from the power laws (Mitchell et al. 1996) for columns, $D \leq 100$ μm. Since these mass power laws were inferred from estimated d_e values, there is every possibility that the actual crystal masses in the cloud chamber were different for a given D than those predicted. Moreover, the length-to-width (i.e., aspect) ratio may naturally vary for a given D, causing mass to vary also. For these reasons, a mass factor was defined, m_f, which multiplies the mass predicted by the mass-D power law. In summary, both m_f and t_f were optimized to yield the minimum error between the measurement derived and predicted Q_{ext}. The m_f for the CS and FSSP was 1.30 and 1.40, respectively. From this information, we were able to derive a width-length power law relation for the columns sampled, which differed from the observed relation reported in Schmitt and Arnott (1999) for similar experimental conditions by only 4% [in Schmitt and Arnott (1999), the length and width was physically measured from the video imagery of the CS].

The optimization procedure is to first assume a t_f of zero and a m_f of 1.0, optimizing first with respect to mass and second with respect to tunneling. The mass optimization sets the basic "pattern" for Q_{ext} (relative minima and maxima), while tunneling controls the amplitude primarily. The program returns estimates of m_f and t_f, and is rerun with these new estimates until the input and output m_f and t_f values are identical (i.e., convergence). Note that t_f is used to calculate $Q_{ext,2\mu m}$ in Eq. (3). No analysis is performed for $x < 1$, where the scheme is not valid.

The results from Method 2 are shown in Figure 5. The average error relative to $Q_{ext,obs}$ was 2.7% for the CS and 3.0% for the FSSP values of $Q_{ext,predicted}$. The optimized tunneling factors for the CS and FSSP were 0.50 and 0.65, respectively. Although these results assumed edge-effect tunneling, repeating this exercise without edge effects made no difference in the results.

Conclusions

Tunneling contributions for hexagonal columns were evaluated in terms of a tunneling factor, t_f, ranging from 0 to 1.0 (i.e., 1.0 corresponding to tunneling predicted by Mie theory for equivalent volume/area spheres). Based on the λ most sensitive to tunneling, $t_f \approx 0.8$, while based on allλ, a t_f range of 0.50 to 0.65 was obtained. These results are qualitatively consistent with theoretical estimates of t_f for prolate spheroids (Baran et al. 1998; $t_f \geq 0.50$) and hexagonal columns (Sun and Fu 1999; Fu et al. 1998; $t_f \geq 0.50$). Since our calculations indicate the sampled columns were solid (not hollow-ended), t_f could be smaller if the columns were hollow.

Our tunneling estimates were not sensitive to whether tunneling due to edge effects was present or not. Therefore, these tunneling estimates pertain to tunneled radiation that enters a particle, and thus can potentially be absorbed, and not to edge-effect tunneling, which does not contribute to absorption (Mitchell 2000). Therefore, the above t_f estimates can be applied to the absorption efficiency, Q_{abs}, as well as Q_{ext}. When these t_f estimates were used in our radiation scheme (Mitchell 1998, 2000), mean errors relative to measured Q_{ext} values in this experiment were ≤ 3.0%.

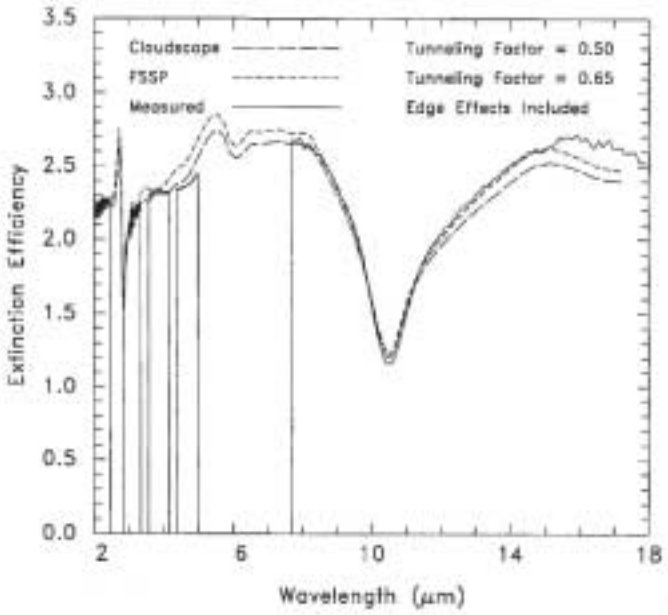

Figure 5. Comparison of measured and predicted Q_{ext} for t_f values that minimize differences based on all wavelengths.

Preliminary experimental estimates of tunneling contributions for hexagonal plates have been made (Mitchell et al. 1999), with mean t_f values being 0.25-0.30. A recent reanalysis of that experiment indicates t_f for plates may be 0.075 to 0.14, although more analysis is warranted. Nonetheless, these estimates for plates are consistent with the theoretical findings (Baran et al. 1998) for oblate spheroids.

Acknowledgment

This work was funded by the Environmental Sciences Division of the U.S. Department of Energy as part of the Atmospheric Radiation Measurement (ARM) Program. The radiation treatment used here is freely available upon request.

Corresponding Author

D. L. Mitchell, 775-674-7039; mitch@dri.edu

References

Arnott, W. P., Y. Dong, and J. Hallett, 1995: Extinction efficiency in the infrared (2-18 μm) of laboratory ice clouds: Observations of scattering minima in the Christiansen bands of ice. *Appl. Opt.*, **34**, 541-551.

Baran, A. J., J. S. Foot, and D. L. Mitchell, 1998: The question of ice crystal absorption: A comparison between T-matrix, Mie and anomalous diffraction theory and implications for remote sensing. *Appl. Opt*., **37**, 2207-2215.

Francis, P. N., J. S. Foot, and A. J. Baran, 1999: Aircraft measurements of the solar and infrared radiative properties of cirrus and their dependence on ice crystal shape. *J. Geophys. Res*., **104**, 31,685-31,695.

Fu, Q., P. Wang, and W. B. Sun, 1998: An accurate parameterization of the infrared radiative properties of cirrus clouds for climate models. *J. Climate*, **11**, 2223-2237.

Guimaraes, L. G., and H. M. Nussenzveig, 1992: Theory of Mie resonances and the ripple fluctuations. *Optics Commun*., **89**, 363-369.

Mitchell, D. L., 1998: Parameterizing the extinction and absorption coefficients in ice clouds: A process oriented approach. Preprints, *Conference on Light Scattering by Nonspherical Particles: Theory, Measurements, and Applications*. AMS, September 29-October 1, New York, pp. 40-43.

Mitchell, D. L., 2000: Parameterization of the Mie extinction and absorption coefficients for water clouds. *J. Atmos. Sci*., **57**, 1311-1326.

Mitchell, D. L., A. Macke, and Y. Liu, 1996: Modeling cirrus clouds. Part II: Treatment of radiative properties. *J. Atmos. Sci*., **53**, 2967-2988.

Mitchell, D. L., W. P. Arnott, C. Schmitt, D. Lowenthal, and J. M. Edwards, 1999: A fundamental difference between ice crystal and cloud droplet absorption: Photon tunneling effects. Preprints, *10th Conf. on Atmospheric Radiation: A Symposium with Tributes to the Works of Verner E. Suomi*, AMS, June 28–July 2, 1999, Madison, Wisconsin.

Nussenzveig, H. M., 1977: The theory of the rainbow. *Sci. Am.*, **236**, 116-127.

Schmitt, C. G., and W. P. Arnott, 1999: Infrared emission (500-2000 cm^{-1}) of laboratory ice clouds. *J. Quant. Spect. Rad. Trans*., **63**, 701-725.

Sun, W., and Q. Fu, 1999: Cirrus spectral brightness temperature in the 8-12 μm window: Theory comparison and remote sensing implication. Preprints, *10th Conf. on Atmospheric Radiation*, AMS, June 28–July 2, 1999, Madison, Wisconsin, pp. 99-102.